Acta Crystallographica Section D
Biological Crystallography
ISSN 0907-4449

An orthorhombic form of *Escherichia coli* aminopeptidase P at 2.4 Å resolution

Stephen C. Graham, Mihwa Lee, Hans C. Freeman and J. Mitchell Guss*

School of Molecular and Microbial Biosciences, University of Sydney, NSW 2006, Australia

Correspondence e-mail: m.guss@mmb.usyd.edu.au

Received 20 January 2002
Accepted 13 March 2003

PDB Reference: orthorhombic AMPP, 1m35, r1m35sf.

Aminopeptidase P (AMPP) from *Escherichia coli* cleaves the N-terminal residue from an oligopeptide if the second residue is proline. The active site contains a dinuclear metal centre. Following earlier structural analyses of crystals in space groups $P6_422$ and $I4_122$, the structure of AMPP has been solved and refined in the orthorhombic space group $C222_1$ at 2.4 Å resolution. There are six subunits in the asymmetric unit. These are arranged in two types of tetramer. One tetramer comprises four crystallographically independent subunits, while the other comprises two pairs of subunits related by a crystallographic twofold axis. The final model of 20 994 protein atoms, 1618 water molecules and 12 metal atoms refined to residuals $R = 0.195$ and $R_{\rm free} = 0.215$. The molecular structure confirms most of the previously reported features, including the subunit–subunit interfaces in the tetramer and persistent disorder at some residues. The metal–ligand bond lengths at the active site suggest that one of the two Mn atoms is five-coordinate rather than six-coordinate.

1. Introduction

Proline forms peptides with secondary instead of the normal primary amide linkages. Thus, cleaving the peptide linkage on the N-terminal side of a proline residue requires a specific type of peptidase. A subset of these enzymes (aminopeptidases P) cleave the N-terminal peptide linkage of peptides and proteins where proline is the second residue. Peptidases specific for dipeptides Xaa-Pro but not longer oligopeptides are termed prolidases. A distinction between the two types of activity was first discovered in extracts of intestinal mucosa (Bergmann & Fruton, 1937) and the structural basis for this distinction is still unknown. Aminopeptidase P (AMPP) has been characterized from a number of mammalian sources, where it is thought to be essential for hormone regulation and regulation of the immune response (Rusu & Yaron, 1992). Mammalian AMPP has been shown to exist in both membrane-bound (Hooper *et al.*, 1990; Ryan *et al.*, 1994; Simmons & Orawski, 1992) and cytosolic forms (Harbeck & Mentlein, 1991; Rusu & Yaron, 1992; Vanhoof *et al.*, 1992). *E. coli* AMPP has been shown to require the presence of Mn^{2+} at pH 8.6 for optimal activity (Yaron & Mlynar, 1968). It has subsequently been shown that the enzyme can be activated in the presence of Co^{2+}, Cd^{2+} and Ni^{2+}, but at significantly lower levels than those achieved in the presence of Mn^{2+} (Yaron & Berger, 1970). Spectroscopic data are consistent with the presence of a dinuclear metal site (Zhang *et al.*, 1998).

AMPP, cloned and overexpressed in *E. coli* as previously reported (Yoshimoto *et al.*, 1988, 1989; Zhang *et al.*, 1998), was originally crystallized in two space groups ($P6_422$ at pH 8.5

and $I4_122$ at pH $\simeq$ 5) and in the presence of a dipeptide inhibitor (Wilce *et al.*, 1998). As predicted from sequence homology (Bazan *et al.*, 1994), the structure was found to be similar to those of the Co-containing methionine aminopeptidase (MetAP) from *E. coli* (Roderick & Matthews, 1993) and the non-metal creatine amidino hydrolase (creatinase) from *Pseudomonas putida* (Hoeffken *et al.*, 1988). In particular, the two metalloenzymes have a dinuclear metal site with identical ligands at the Mn atoms in AMPP and the Co atoms in MetAP. The functional form of AMPP under physiological conditions is probably a tetramer and this is the form found in the crystals (Wilce *et al.*, 1998). Each subunit of the tetramer has two domains. The larger C-terminal domain contains the dinuclear Mn centre. In the hexagonal and tetragonal crystal forms the asymmetric unit consists of a single subunit and the tetramers have crystallographic 222 symmetry. AMPP has now been crystallized in an orthorhombic space group with six subunits in the asymmetric unit.

2. Experimental

2.1. Crystallization

AMPP was cloned and expressed as described previously (Wilce *et al.*, 1998) using a modification of a published method (Yoshimoto *et al.*, 1989). Briefly, AMPP was overexpressed in *E. coli* AN1459/pPL670. Lysed cells were subjected to ammonium sulfate precipitation at 277 K followed by centrifugation. The pellet was resuspended and applied to a DEAE-Fractogel column (Merck). The AMPP-containing fraction was then passed over a ceramic hydroxyapatite column (Bio-Rad). Crystals were grown by the method of vapour diffusion in hanging drops. A drop containing 3 µl of protein solution (8 mg ml^{-1} in 20 m*M* Tris buffer pH 8.5) was mixed with 2 µl of reservoir solution (25% PEG 4000, 0.1 *M* Tris–HCl, 0.2 *M* sodium acetate pH 8.0) and 0.55 µl of 10 m*M* $MnCl_2$ (giving a final $MnCl_2$ concentration of 1 m*M*). Crystals grew to maximum dimensions of approximately 0.5 × 0.3 × 0.1 mm in one month at 277 K. Crystals were prepared for flash-freezing by transferring them successively to reservoir solutions containing 5 and 10% methylpentanediol and were left in the cryoprotectant solution for 48 h at 277 K.

2.2. Synchrotron data

X-ray diffraction data were recorded at the Stanford Synchrotron Radiation Laboratory on beamline 7-1 with an X-ray wavelength of 1.08 Å at 100 K. An X-ray Research MAR345 imaging-plate detector was placed 300 mm from the crystal, giving a nominal resolution of 2.1 Å at the edge of the plate. A total of 299 successive images were recorded with an oscillation angle of 0.35°, giving a total angular coverage of 104.7° and an overall redundancy of 4.2.

2.3. Structure solution

AMPP was assumed to be a tetramer. The fact that space group $C222_1$ has no positions with point symmetry 222 implies that there is an even number of molecules in the asymmetric unit. The solvent content of the crystals was consistent with either eight molecules (two tetramers), six molecules (1.5 tetramers) or four molecules (one tetramer) in the asymmetric unit: estimates of the solvent content (Matthews, 1968) were 64% for two tetramers per asymmetric unit, 73% for 1.5 tetramers and 82% for one tetramer per asymmetric unit. In the previously observed crystal forms of AMPP the solvent contents were 72 and 80%, respectively.

A self-rotation function (not shown) revealed two non-crystallographic twofold axes perpendicular to the crystallographic z axis. Examination of the refined structure subsequently showed two other local twofold axes parallel to the x and z axes, which were masked by crystallographic symmetry in the self-rotation function.

An AMPP tetramer from the structure in space group $P6_422$ (PDB entry 1az9; Wilce *et al.*, 1998), minus Mn^{2+} ions and solvent molecules, was used as the search model for calculating a cross-rotation function (data range 40–4 Å, integration radius 40 Å). Two solutions had correlation coefficients more than twice as large as that of the next solution. The solution with the largest coefficient was used in a translation search, yielding the orientation and position of one tetramer within the unit cell. This solution was provisionally accepted and was used in a translation search with the second-best solution of the rotation function. This located a second tetramer. The first tetramer was found to lie across the crystallographic twofold axis parallel to z, while the second was in a general position.

2.4. Structure refinement

Initial rigid-body refinement with all data to 4 Å resolution resulted in residuals $R = 0.286$ and $R_{\rm free} = 0.292$. Phases were extended to the limit of the data, 2.4 Å, by averaging and solvent flattening using an input mask created from a monomer of the AMPP search model. The phases were averaged using the sixfold non-crystallographic symmetry in the asymmetric unit. $F_o - F_c$ and $3F_o - 2F_c$ electron-density difference maps assisted manual model rebuilding. The two metal atoms at the active site, having been omitted from the initial model, were identified in the first difference Fourier synthesis as peaks exceeding 10σ. Several rounds of model building, including the addition of solvent molecules, were interspersed with simulated annealing at 4000 K. Initially, each amino-acid residue was treated as two groups of atoms with independent temperature parameters. In the final stages of refinement, Arg, Lys, Gln and Glu residues were treated as three groups of atoms. The first group comprised the backbone atoms. For Glu and Gln, the second group consisted of the atoms C^{β} and C^{γ}, and the third group consisted of all atoms beyond C^{γ}. For Arg and Lys, the second group consisted of the atoms C^{β}, C^{γ} and C^{δ}, and the third group consisted of atoms beyond C^{δ}.

Non-crystallographic symmetry (NCS) restraints were imposed throughout the refinement. At the start of the refinement the NCS was imposed rigorously (constrained),

Table 1
Data and refinement statistics for orthorhombic AMPP.

Values in parentheses refer to the highest resolution shell.

Space group	$C222_1$
Unit-cell parameters (Å)	
a	209.1
b	314.0
c	162.0
Resolution range (Å)	20.0–2.4 (2.51–2.40)
No. of unique reflections	197708
Redundancy	4.2 (3.8)
Completeness (%)	95.7 (87.7)
$\langle I/\sigma(I)\rangle$	22.7 (4.1)
$R_{\rm merge}$	0.058 (0.30)
Reflections used in refinement	197455
Reflections in test set	9679
No. of atoms	
Protein (excluding H atoms)	20994
Solvent	1618
Metal ions	12
R	0.195 (0.263)
$R_{\rm free}$	0.215 (0.292)
R.m.s.d. from bond ideality (Å)	0.006
R.m.s.d. from angle ideality (°)	1.3
DPI (Å)	0.28

one subunit being used to generate the other five by the application of appropriate transformation matrices. The rigorous NCS constraints were later relaxed to strong restraints [weight = 100, target $\sigma(B) = 2$]. NCS restraints were only applied to those 2503 residues that were located in well resolved density in all six subunits and that were not involved in any tetramer–tetramer contact. Some residues remained consistently poorly defined in all independent subunits: residues 85–89, residue 243 and the C-terminal residues 439–440. At the end of the refinement, 35 residues in the asymmetric unit that were unrestrained were located in weak electron density and had temperature factors with the maximum permitted value, $B_{\rm max} = 100$ Å^2. One or more side-chain atoms of a further 102 residues were also located in weak electron density and their temperature factors refined to values of 100 Å^2. These residues were included in the model with high temperature factors to reduce the volume available to bulk solvent.

Water molecules were added using an automatic script based on geometry (distance $\leq$3.5 Å to plausible hydrogen-bonding partner) and peaks (>4.5σ) in difference electron-density maps. Putative solvent molecules with real-space correlation coefficients (Jones *et al.*, 1991; Kleywegt & Jones, 1997*a*) below 0.8 in $3F_o - 2F_c$ electron-density maps were deleted. After the final refinement cycle the residuals were $R = 0.195$ and $R_{\rm free} = 0.215$[1]. The results of the data collection and refinement are summarized in Table 1.

2.5. Quality of the model

A Ramachandran plot (not shown) computed from the final model has all but one amino-acid residue in each polypeptide chain in allowed regions. The outlier is Ala37, which has the same conformation in each of the six independent polypeptide chains and is the same in structures of AMPP refined in other space groups (Wilce *et al.*, 1998). The coordinate errors as estimated from the diffraction precision indicator (Cruickshank, 1999) and from σ_A plots (Read, 1986, 1990) are 0.28 and 0.31 Å, respectively. The model includes all the protein atoms, but parts of some residues are in weak electron density and their thermal parameters have refined to relatively high values.

2.6. Software

The integrated intensities were obtained using *DENZO* from the *HKL* suite (Otwinowski & Minor, 1997). The data were merged and scaled with *SCALEPACK*. The self-rotation function was calculated using *POLARRFN* (Collaborative Computational Project, Number 4, 1994). *AMoRe* (Navaza, 1994) was used for the cross-rotational and translational searches. All model fitting was performed using *O* (Jones *et al.*, 1991). *REFMAC*5 (Murshudov *et al.*, 1997) was used for initial rigid-body refinement. *DM* (Cowtan, 1994) was used to perform averaging and solvent flattening. The *CNS* (Brünger *et al.*, 1998) suite was used for the refinement process. All surface areas were calculated using the *CCP*4 program *AREAIMOL* (Lee & Richards, 1971) with a point density of 100 points per Å^2. Root-mean-square distances between C$^\alpha$ atoms were calculated using *LSQMAN* (Kleywegt & Jones,

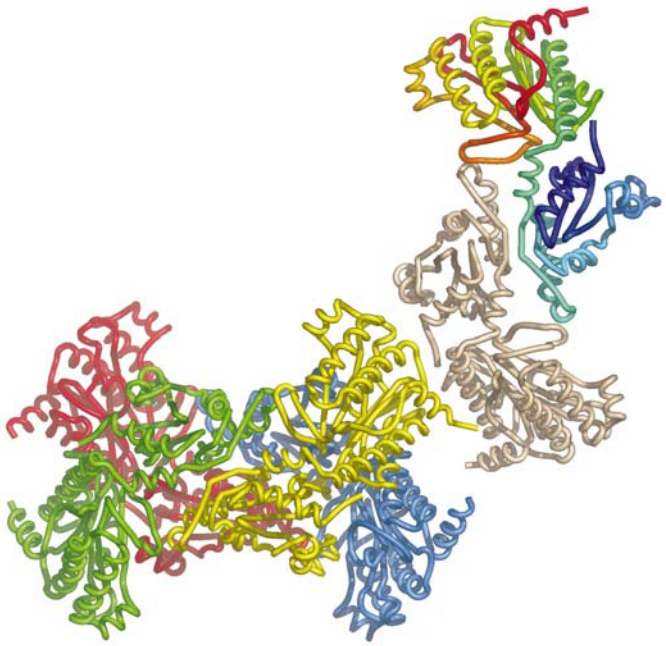

Figure 1
Projection of the six independent subunits in the asymmetric unit of orthorhombic AMPP. The red, green, blue and yellow subunits form a tetramer with approximate (non-crystallographic) 222 symmetry. The remaining subunits are half of a second tetramer formed by the operation of a crystallographic twofold parallel to the vertical edge of the paper. The colour in the one of these subunits has been ramped from blue at the N-terminus to red at the C-terminus to facilitate the distinction between the domains.

[1] Since the test set of reflections was not chosen in thin shells, there is the possibility of bias in the value of $R_{\rm free}$ introduced by the non-crystallographic symmetry (Kleywegt & Jones, 1995), but the effect on the refinement is likely to be negligible (Kleywegt & Brünger, 1996).

Table 2
Root-mean-square differences (Å) between C^{α} atom positions when pairs of subunits are superposed.

ABCDEF, subunits in the orthorhombic structure (present work). Hexagonal, PDB code 1az9. Tetragonal, PDB code 1jaw.

Subunit or crystal form	*A*	*B*	*C*	*D*	*E*	*F*	Hexagonal
B	0.21	—					
C	0.10	0.23	—				
D	0.14	0.15	0.15	—			
E	0.20	0.15	0.23	0.16	—		
F	0.09	0.17	0.12	0.12	0.17	—	
Hexagonal	0.33	0.41	0.32	0.38	0.39	0.33	—
Tetragonal	0.27	0.38	0.27	0.33	0.36	0.30	0.32

1997*b*). The two C-terminal residues 439 and 440, which do not adopt a single conformation, were omitted from all superpositions.

Table 3
Manganese–ligand distances in AMPP.

The values listed under 'orthorhombic' are the ranges in the six subunits in the asymmetric unit (present work). The values listed under 'hexagonal' are from the previously published structure (Wilce *et al.*, 1998).

	Orthorhombic		Hexagonal	
Ligand	Mn_A	Mn_B	Mn_A	Mn_B
Asp260 $O^{\delta1}$		2.18–2.31		2.09
Asp260 $O^{\delta2}$		2.24–2.29		2.38
Asp271 $O^{\delta1}$		1.98–2.06		2.03
Asp271 $O^{\delta2}$	1.91–1.97		2.09	
His354 $N^{\varepsilon2}$	2.08–2.17		2.18	
Glu383 $O^{\varepsilon1}$	2.20–2.25		2.15	
Glu406 $O^{\varepsilon1}$		2.11–2.18		2.19
Glu406 $O^{\varepsilon2}$	2.05–2.15		2.15	
W1	1.97–2.18	1.89–2.09	2.07	2.21
W2	3.04–3.51		2.84	
W3		2.32–2.68		2.37
Mn_B or Mn_A	3.12–3.26	3.29		

3. Results and discussion

In a general sense, the present work confirms the correctness of the molecular structures of AMPP at pH 8.5 (hexagonal crystals) and pH $\simeq$ 5 (tetragonal crystals; Wilce *et al.*, 1998). In the previous structures, the four subunits of the tetramer were related by crystallographic symmetry. In the present work there are two types of tetramer in the asymmetric unit, one comprising four crystallographically independent subunits and the other comprising two crystallographically independent dimers related by a twofold axis (Fig. 1). The subunit–subunit contacts in all the structures are similar, involving either a pair of N-terminal domains or a pair of C-terminal domains. The buried area is $\sim$625 Å^2 per subunit in the former contacts and $\sim$2100 Å^2 per subunit in the latter contacts, compared with a total solvent-accessible surface area of $\sim$20 000 Å^2 per subunit.

When the six crystallographically independent subunits are superposed upon one another and upon the two previously determined structures, the root-mean-square deviations between the positions of corresponding C^{α} atoms are always in the range 0.1–0.4 Å (Table 2). While this shows that the subunit structure is conserved, the present refinement confirms earlier evidence (Wilce *et al.*, 1998) that several residues within the molecule are significantly disordered. As stated in §2.4, the disorder was indicated both by conformational differences between the subunits and by very high temperature factors at the end of the refinement. The relative independence of molecular structure from crystallization conditions is confirmed by the finding that at least 77 solvent sites per subunit are conserved in each subunit of the present structure as well as the previously reported high-pH and low-pH forms.

The present work suggests that the dinuclear metal site is not as symmetrical as previously reported. Instead of two six-coordinate Mn atoms, the active site in the present structure appears to have one five-coordinate and one six-coordinate Mn atom. The Mn_A-OH_2 distance, $\sim$3.2 Å (Table 3), is only slightly greater than that reported previously (2.8 Å; Wilce *et al.*, 1998). There appears to be insufficient room to accommodate an additional water molecule to complete an octahedral coordination sphere around Mn_A, but given the resolution of the structure refinement some disorder of the solvent structure cannot be discounted. The coordination geometry of Mn_A is then best described as square pyramidal, while that of Mn_B remains approximately octahedral. A geometrical difference between the two metal-atom geometries would be consistent with increasing evidence that the two metal atoms differ in binding constant and catalytic efficacy in related enzymes. In MetAP and mammalian aminopeptidases P, the identity and number of metal atoms in the active form remain uncertain. It has been suggested that MetAP is in fact a Zn or Fe enzyme (D'Souza & Holz, 1999; Walker & Bradshaw, 1998), that human cytosolic AMPP can function with a single Mn atom (Cottrell, Hooper *et al.*, 2000) and that the porcine membrane-bound AMPP contains a single Zn ion (Cottrell, Hyde *et al.*, 2000).

The present results are relevant to several other aspects of the active site. It has been suggested that

> the conserved residues His243 [and] His350 . . . may shuttle protons from the dinuclear center to the solvent

(Wilce *et al.*, 1998). In the case of His243, an involvement in the catalytic mechanism is supported by the recent observation that a mutation of the corresponding residue, His79, in MetAP reduces the catalytic activity by five orders of magnitude (Lowther *et al.*, 1999). While the precise function of His243 in the catalytic mechanism is not yet known, a high degree of mobility of this residue is indicated by the side-chain disorder, which was previously reported and is found again in the present structure.

The hypothesis that His350 is part of a functionally important proton-transfer chain (Wilce *et al.*, 1998) requires modification. His350 lies on a bulge in a β-strand (residues 347–356), which is antiparallel to another β-strand (residues 379–387). If the His350 imidazole ring is modelled in its original orientation, it can form at best one weak hydrogen

bond (3.1 Å) to the O(peptide) of Glu383. If the imidazole ring is rotated from that orientation by 180° about the $C^{\beta}-C^{\gamma}$ bond, it can form two strong hydrogen bonds (Fig. 2). The first, from the $N^{\delta1}$ atom to the O(peptide) of the adjacent residue Gly351 (2.8 Å), stabilizes the orientation of the imidazole ring. The second links the imidazole $N^{\varepsilon2}$ atom to the O^{η} atom of Tyr387 on the adjacent β-strand (2.7 Å). Both His350 and Tyr387 are four residues removed from an Mn-binding residue. His354, the fourth residue in the C-terminal direction from His350, and Glu383, the fourth residue in the N-terminal direction from Tyr387, are both coordinated to active-site Mn_A. Thus, if His350 has a function at all, it is likely to be stabilization of the active-site environment.

The previously reported but unexplained observation of an unusual backbone conformation at Ala37 is confirmed. Fig. 3 is an example of the strong electron density at Ala37 in all six crystallographically independent subunits of the present model. The φ and ψ angles (49.3–50.6, −120.3 to −118.6°) lie just outside the 'additionally allowed' region of the Ramachandran plot. Ala37 is the second residue of a type II′ β-hairpin turn located at the end of a 'finger' pointing from one subunit towards the active site of another. The sequence in the turn is Ser36-Ala37-Asp38-Ser39. The Gly expected at the second position of a canonical type II′ turn (Wilmot & Thornton, 1990) has been replaced by Ala. In the Ramachandran plot, Ala37 occupies a position that would be acceptable for Gly but is less so for Ala. The C^{β} of Ala37 makes no close contacts and there is no obvious explanation why it is present in place of Gly. The formation of the β-hairpin enables the carboxylate group of Asp38 to form a hydrogen bond to the side chain of His361 in the adjacent subunit. This may stabilize the orientation of the imidazole ring of His361, which is located in the active-site cavity, but implies that the imidazole ring is protonated at $N^{\delta1}$. Thus, a proposed enzyme mechanism, in which His361 is protonated at $N^{\varepsilon2}$ and stabilizes an oxyanion intermediate (Fig. 3 of Wilce

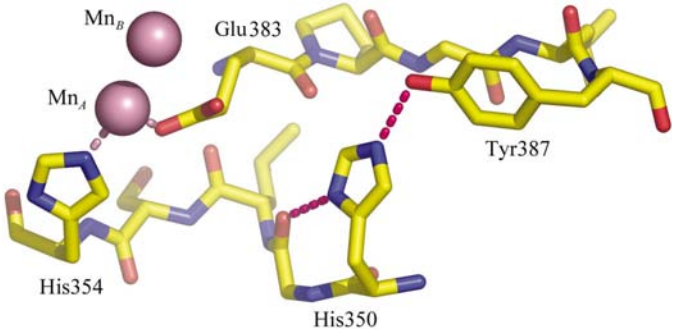

Figure 2
A preferred orientation of the imidazole ring of His350, showing hydrogen bonds to the O(peptide) of His351 and to the O^{η} of Tyr387. Two nearby ligands of Mn_A and their interactions with the metal are also shown.

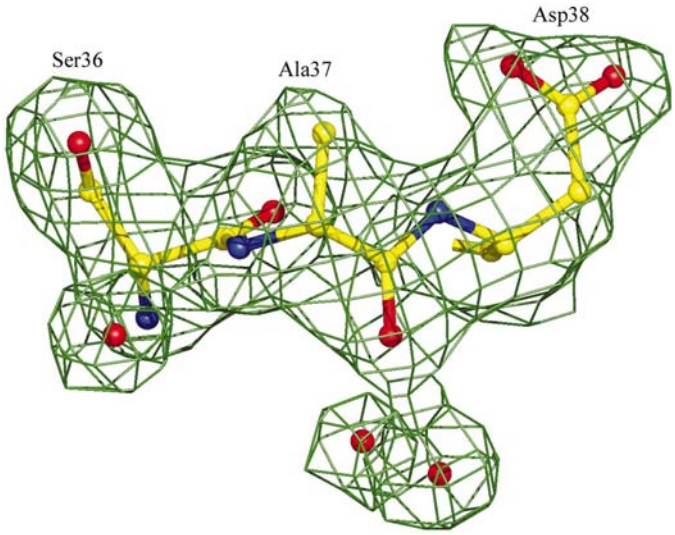

Figure 3
Electron density (4.5σ) at the strained residue Ala37. The $F_o - F_c$ electron-density difference map was calculated after energy minimization without NCS restraints and omitting Ala37 and all residues within 3.5 Å from F_c.

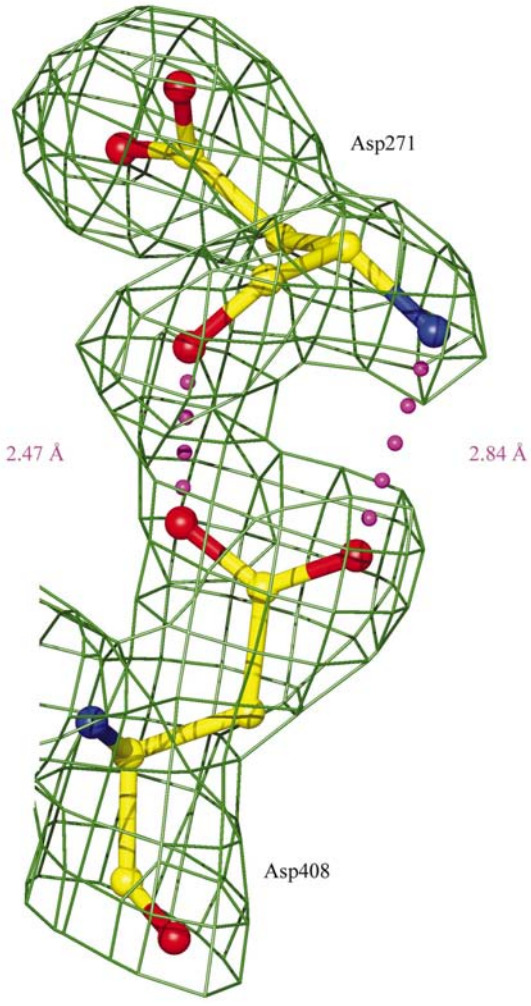

Figure 4
A protonated side chain at Asp408. The carboxyl group of Asp408 makes hydrogen bonds with backbone O(peptide) and N(peptide) atoms of the active-site ligand Asp271. The $F_o - F_c$ electron-density difference (5.0σ) was calculated after energy minimization without NCS restraints and omitting Asp408 and all residues within 3.5 Å from F_c.

et al., 1998), may require reconsideration. Nonetheless, His361 is likely to have functional importance since it is conserved in AMPP across species and in the related enzymes MetAP and prolidase. A His→Ala mutation of the equivalent residue in MetAP leads to a 50-fold drop in enzymatic activity (Lowther *et al.*, 1999).

A structural feature not noted previously but shared by all AMPP structures is a close approach between the carboxyl group of Asp408 and the protein backbone (Fig. 4). The $O^{\delta1}$ and $O^{\delta2}$ atoms of Asp408 make contacts of 2.5 and 2.9 Å, respectively, with the O(peptide) and N(peptide) atoms of Asp271. Both contacts must be hydrogen bonds, implying that the carboxyl group is protonated. The side chain of Asp408 is not solvent-accessible. The protonation of carboxyl groups in hydrophobic environments has been noted, for example, in β-lactamase (Swaren *et al.*, 1995).

4. Conclusions

Refinement of the structure of a new crystal form of AMPP with six molecules in the asymmetric unit confirms the previously reported quaternary structure of the tetrameric molecule and the tertiary structure of the independent subunits. There is evidence that the dinuclear Mn site has one five-coordinate and one six-coordinate metal atom. A number of structural features that may be related to the function of the enzyme are discussed.

This research was supported by grant DP0209273 from the Australian Research Council (JMG and HCF). SCG is supported by an Australian Postgraduate Award. Access to the Stanford Synchrotron Radiation Laboratory was supported by a travel grant from the Access to Major Research Facilities Program administered by the Australian Nuclear Science and Technology Organization.

References

Bazan, J. F., Weaver, L. H., Roderick, S. L., Huber, R. & Matthews, B. W. (1994). *Proc. Natl Acad. Sci. USA*, **91**, 2473–2477.
Bergmann, M. & Fruton, J. S. (1937). *J. Biol. Chem.* **117**, 189–202.
Brünger, A. T., Adams, P. D., Clore, G. M., DeLano, W. L., Gros, P., Grosse-Kunstleve, R. W., Jiang, J. S., Kuszewski, J., Nilges, M., Pannu, N. S., Read, R. J., Rice, L. M., Simonson, T. & Warren, G. L. (1998). *Acta Cryst.* D**54**, 905–921.
Collaborative Computational Project, Number 4 (1994). *Acta Cryst.* D**50**, 760–763.
Cottrell, G. S., Hooper, N. M. & Turner, A. J. (2000). *Biochemistry*, **39**, 15121–15128.
Cottrell, G. S., Hyde, R. J., Lim, J., Parsons, M. R., Hooper, N. M. & Turner, A. J. (2000). *Biochemistry*, **39**, 15129–15135.
Cowtan, K. (1994). *Jnt CCP4/ESF–EACBM Newsl. Protein Crystallogr.* **31**, 34–38.
Cruickshank, D. W. J. (1999). *Acta Cryst.* D**55**, 583–601.
D'Souza, V. M. & Holz, R. C. (1999). *Biochemistry*, **38**, 11079–11085.
Harbeck, H. T. & Mentlein, R. (1991). *Eur. J. Biochem.* **198**, 451–458.
Hoeffken, H. W., Knof, S. H., Bartlett, P. A. & Huber, R. (1988). *J. Mol. Biol.* **204**, 417–433.
Hooper, N. M., Hryszko, J. & Turner, A. J. (1990). *Biochem. J.* **267**, 509–515.
Jones, T. A., Zou, J. Y., Cowan, S. W. & Kjeldgaard, M. (1991). *Acta Cryst.* A**47**, 110–119.
Kleywegt, G. J. & Brünger, A. T. (1996). *Structure*, **4**, 897–904.
Kleywegt, G. J. & Jones, T. A. (1995). *Structure*, **3**, 535–540.
Kleywegt, G. J. & Jones, T. A. (1997*a*). *Methods Enzymol.* **277**, 208–230.
Kleywegt, G. J. & Jones, T. A. (1997*b*). *Methods Enzymol.* **277**, 525–545.
Lee, B. & Richards, F. M. (1971). *J. Mol. Biol.* **55**, 379–400.
Lowther, W. T., Orville, A. M., Madden, D. T., Lim, S., Rich, D. H. & Matthews, B. W. (1999). *Biochemistry*, **38**, 7678–7688.
Matthews, B. W. (1968). *J. Mol. Biol.* **33**, 491–497.
Murshudov, G. N., Vagin, A. A. & Dodson, E. J. (1997). *Acta Cryst.* D**53**, 240–255.
Navaza, J. (1994). *Acta Cryst.* A**50**, 157–163.
Otwinowski, Z. & Minor, W. (1997). *Methods Enzymol.* **276**, 307–326.
Read, R. J. (1986). *Acta Cryst.* A**42**, 140–149.
Read, R. J. (1990). *Acta Cryst.* A**46**, 900–912.
Roderick, S. L. & Matthews, B. W. (1993). *Biochemistry*, **32**, 3907–3912.
Rusu, I. & Yaron, A. (1992). *Eur. J. Biochem.* **210**, 93–100.
Ryan, J. W., Denslow, N. D., Greenwald, J. A. & Rogoff, M. A. (1994). *Biochem. Biophys. Res. Commun.* **205**, 1796–1802.
Simmons, W. H. & Orawski, A. T. (1992). *J. Biol. Chem.* **267**, 4897–4903.
Swaren, P., Maveyraud, L., Guillet, V., Masson, J. M., Mourey, L. & Samama, J. P. (1995). *Structure*, **3**, 603–613.
Vanhoof, G., De Meester, I., Goossens, F., Hendriks, D., Scharpe, S. & Yaron, A. (1992). *Biochem. Pharmacol.* **44**, 479–487.
Walker, K. W. & Bradshaw, R. A. (1998). *Protein Sci.* **7**, 2684–2687.
Wilce, M. C. J., Bond, C. S., Dixon, N. E., Freeman, H. C., Guss, J. M., Lilley, P. E. & Wilce, J. A. (1998). *Proc. Natl Acad. Sci. USA*, **95**, 3472–3477.
Wilmot, C. M. & Thornton, J. M. (1990). *Protein Eng.* **3**, 479–493.
Yaron, A. & Berger, A. (1970). *Methods Enzymol.* **19**, 521–534.
Yaron, A. & Mlynar, D. (1968). *Biochem. Biophys. Res. Commun.* **32**, 658–663.
Yoshimoto, T., Murayama, N., Honda, T., Tone, H. & Tsuru, D. (1988). *J. Biochem. (Tokyo)*, **104**, 93–97.
Yoshimoto, T., Tone, H., Honda, T., Osatomi, K., Kobayashi, K. & Tsuru, D. (1989). *J. Biochem. (Tokyo)*, **105**, 412–416.
Zhang, L., Crossley, M. J., Dixon, N. E., Ellis, P. J., Fisher, M. L., King, G. F., Lilley, P. E., MacLachlan, D., Pace, R. J. & Freeman, H. C. (1998). *J. Biol. Inorg. Chem.* **3**, 470–483.